

Evaluation of Hip Kinematics Influence on the Performance of a Quadrupedal Robot Leg

Navvab Kashiri, Arash Ajoudani, Darwin G. Caldwell and Nikos G. Tsagarakis

Department of Advanced Robotics, Istituto Italiano di Tecnologia, Via Morego 30, 16163 Genova, Italy

Keywords: Leg Kinematics Design, Quadrupeds, Legged Robots, Force Manipulability/Polytope, Dynamic Manipulability/Polytope.

Abstract: As a major inspiration of biologically inspired systems, multi-legged robots have been developed due to their superior stability feature resulting from their large support polygon. The leg design of a majority of such robots is motivated by the skeleton of vertebrates such as dogs, or that of invertebrates such as spiders. Despite a wide variety of multi-pedal robots on the basis of the two aforesaid leg designs, a thorough comparison of the two underlying design principles remains to be done. This work addresses this problem and presents a comparative study for the two mammal-like and spider-like designs by looking at the joint torque profile, the responsive motion of the legs, and the thrust force applied by the robot. To this end, a set of performance indexes are defined based on the gravity compensation torque, the dynamic manipulability polytope and the force polytope, and evaluated in various leg configurations of the two designs.

1 INTRODUCTION

Robots have been widely employed in industrial settings during the past four decades, offering a range of functionality from manufacturing to food processing. While a majority of such platforms are manipulators mounted on fixed/wheeled bases, there are many scenarios that the robot needs to operate in complex, unstructured, and dynamically changing environments, where the human-/animal-like degrees of mobility and agility would be essential (Caldwell et al., 2014). Such a demand has created new opportunities for the legged robots whose functionality is not limited to naturally or artificially smoothed terrains. Hence, an increasing worldwide attention has been given to the development of pedal robots within the past decade.

Even though the underlying anthropomorphic structure of humanoid robots has illustrated the potential of generating human-like mobility and manipulation skills (Negrello et al., 2016; Bagheri et al., 2015), the control of balance while performing highly dynamic tasks or walking along rough terrains is troublesome and still appears in a developing stage. Multi-pedal robots (e.g. quadrupeds and hexapods), on the other hand, present a higher level of balancing performance due to a larger support polygon compared to the bipedal ones.

The BigDog quadrupeds (Raibert et al., 2008) developed by the Boston Dynamics, Inc., is a renowned example of walking robots built for outdoor applications, whose design is inspired by the skeleton of mammals. The StarLETH (Hutter et al., 2012), LittleDog (Shkolnik et al., 2010), XDOG (Xie et al., 2014), MIT Cheetah (Seok et al., 2013), IIT HyQ (Semini et al., 2011) and Cheetah-cub (Spröwitz et al., 2013) are other examples of quadrupeds motivated by the mammalian morphology. Alternative design of the robot legs is inspired by the leg structure of insects and arachnids such as spider (Ho et al., 2007; Gasparetto et al., 2008), examples of which can be found in the design of TITAN quadruped (Kato and Hirose, 2001), LAVA (Zielinska and Heng, 2003), LAURON V (Roennau et al., 2013), PUT Hexapod Robots (Belter et al., 2015), MRWALLSPECT-III (Kang et al., 2003), and MiniQuad I (Chen et al., 2008).

Despite the fast growing interest in the application of the quadruped robots in various real-world scenarios, the literature still fails to present a through comparative study for the two aforementioned design principles, especially regarding the dynamic capabilities of the robot. Previous work in this area mainly concerns kinematic considerations (Kar, 2003; Chen et al., 2006; Zielinska, 2013), e.g. analysis of the optimum inclination angle of the hip joint on the

basis of kinematics manipulability (Roennau et al., 2013). With that being said, this paper will attempt to present a deeper analysis of the mammal-like and spider-like legs for quadrupedal robots, although it can be exploited for other pedal platforms in a similar fashion. In this direction, a group of indexes describing the statics and dynamics of the robot is defined and evaluated throughout the workspace of the robot. The proposed indexes are based on three criteria: the torque capacity computed from the gravity compensation torque of joints representing the static energy consumption of the system; a set of measures derived from the dynamic manipulability of legs describing the reactive capabilities of the robot; and others extracted from the force manipulability of legs analysing the capabilities of the robot to avoid slippage. The study of the force/dynamic manipulability is achieved through the definition of the corresponding polytopes (Chiacchio et al., 1997), to present the exact boundaries of the manipulator in a given configuration, subject to the actuator torque bounds, in comparison to alternative less-accurate representations such as ellipsoids (Yoshikawa, 1985).

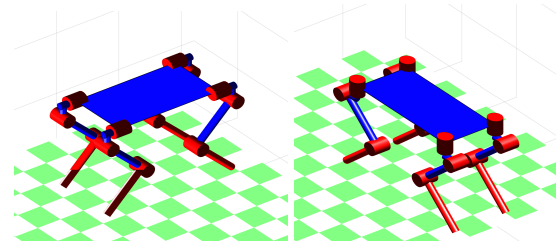
The rest of this paper is organized as follows: Section II describes the problem to be discussed in this paper. The corresponding formulation is presented in Section III, including the kinematics and dynamics background, and the elaboration of the three groups of criteria utilised for this comparison study. Simulation analysis of the two mammal/spider-like leg design quadrupeds are illustrated in Section IV, and the pertinent results are discussed. Finally, Section V addresses the conclusion and future works.

2 PROBLEM STATEMENT

A majority of quadrupedal robots make use of two pre-dominant kinematics arrangements inspired by the mammal or spider type legs, as noted in the literature review. Concerning the first three joints of the leg related to the hip and the knee, they can be described as follows

- mammal-like legs: A roll hip joint permitting the abduction/Adduction motion is used for the first joint, in addition to two pitch joints for generating flexion/extension motion of hip and knee joints.
- spider-like legs: A yaw joint replicating medial/lateral rotation is implemented on the first joint, followed by two pitch joints similar to mammal-like arrangement.

The Schematics of quadrupeds with these two leg



(a) Roll-Pitch-Pitch leg (b) Yaw-Pitch-Pitch leg

Figure 1: Schematics of the two conventional kinematics arrangement of quadrupedal robots. (The above images are generated by means of the Matlab Robotics Toolbox (Corke, 2011)).

arrangements are shown in Fig. 1. In this work, the problem is set to realize the evolution of statics and dynamics of these two types of quadrupedal robots, so that the functionality of such robots for various scenarios can be understood.

3 PROBLEM FORMULATION

3.1 Kinematics and Dynamics Background

In this section the rigid body kinematics and dynamics of non-redundant robotic linkages are briefly reported, see (Siciliano et al., 2009) for details. For a given n -link body, the kinematic relation expressing the end-effector position in the task space based on joint coordinates can be expressed by a vector function $\mathbf{r} \in \mathcal{R}^n$ as follows¹

$$\mathbf{p} = \mathbf{r}(\mathbf{q}), \quad (1)$$

$$\dot{\mathbf{p}} = \mathbf{J}(\mathbf{q})\dot{\mathbf{q}}, \quad (2)$$

where $\mathbf{J} \in \mathcal{R}^{n \times n}$ is the velocity Jacobian matrix, defined by $\mathbf{J} = \frac{\partial \mathbf{r}(\mathbf{q})}{\partial \mathbf{q}}$, $\mathbf{p} \in \mathcal{R}^n$ represents the end-effector position in the task space, and the superscript “ T ” denotes the transpose operator. The governing differential equations of this dynamical system can be expressed by

$$\mathbf{M}(\mathbf{q})\ddot{\mathbf{q}} + \mathbf{C}(\mathbf{q}, \dot{\mathbf{q}})\dot{\mathbf{q}} + \mathbf{g}(\mathbf{q}) = \boldsymbol{\tau}_m - \mathbf{J}^T \mathbf{F}_{ext}, \quad (3)$$

where $\mathbf{M}(\mathbf{q}) \in \mathcal{R}^{n \times n}$ is the inertia matrices associated with links; $\mathbf{q} = [q_1, \dots, q_n]$ shows the vector of generalized link positions; $\mathbf{F}_{ext} \in \mathcal{R}^n$ is the vector of forces applied by external objects/agents, $\boldsymbol{\tau}_m \in \mathcal{R}^n$ represents the vector of torques exerted by motors; $\mathbf{C}(\mathbf{q}, \dot{\mathbf{q}})\dot{\mathbf{q}} \in \mathcal{R}^n$ and $\mathbf{g}(\mathbf{q}) \in \mathcal{R}^n$ denote vectors of Coriolis/centrifugal and gravitational torques of the links, respectively.

¹Newton’s notation (over-dot) is used in this paper for the presentation of derivatives with respect to time.

3.2 Torque Capacity Measure: Gravity Compensation Torque

The first criterion on the leg design analysis is the joints torques required in static conditions. Hence, the robot is positioned in different configurations within its workspace, and the gravity compensation torques of joints are analysed. The maximum torque of each joint required for holding the robot in position, which is an essential measure for the design, is therefore extracted. The evaluation is carried out in two cases, when the robot stands on a flat surface and on an inclined surface. For the sake of simplicity, legs are assumed be in mutually symmetrical postures with respect to principal planes described by XYZ -coordinate system, as shown in Fig. 2(b). When the robot is positioned on a horizontal plane, i.e. the surface slope $\gamma = 0$, the main body mass is equally distributed between the four legs. However, when the robot stand on an inclined surface with a slope of γ , as shown in Fig. 2(a), the ground reaction force applied on rear legs F_r will be larger than that on front legs F_f for typical slope angles $0 \leq \gamma \leq 30^\circ$. The rear leg gravity compensation torque is thus used for the torque capacity evaluations.

3.3 Responsive Motion Index: Dynamic Manipulability Polytope

For a given scenario in which the robot is subject to external disturbances, the balance recovery requires the placement of foot to right place using various techniques (Pratt and Tadrake, 2006). The responsive motions of the leg therefore plays a significant role in balancing of it, as well as in dynamic motions of the robot. In order to evaluate the agility of the robot in execution of such motions, the dynamic manipulability concept is exploited. According to the definition of the dynamic manipulability, proposed and elaborated in (Yoshikawa, 1985), this index is described on the basis of the relation between the joint driving torque and the end-effector acceleration, and it represents the robot capability of producing

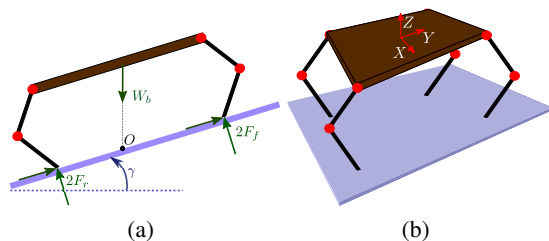


Figure 2: Schematics of the quadrupedal robot to be discussed in this work, without demonstrating the first joint of the leg (hip yaw/roll).

arbitrary accelerations at the end-effector. To this end, the dynamic manipulability polytope (DMP) is exploited in this work to account for the exact acceleration boundaries of the leg in task space, so that the dynamic capability of legs in generating instantaneous responsive motions can be precisely illustrated. Since the main leg movement required for the balance recovery of the robot should be carried out within the plane in parallel to the ground, the dynamic manipulability evolution in this plane will mostly be focused, although the variation of this criterion in vertical axis will also be evaluated.

To define the DMP, the joint torque polytope defining $2n$ bounds are expressed as follows

$$|\tau_m| \leq \tau_{max} \quad (4)$$

where τ_{max} is the vector of maximum joint torques, and $|\cdot|$ symbolizes the absolute value operator acting on the components of the vector.

The DMP can therefore be derived by mapping the vertices of the joint torque polytope. As it was studied in (Yoshikawa, 1985; Chiacchio et al., 1997), the mapping relation is extracted from (3) and the second time derivative of (1) when assuming the robot is standing still. It can therefore be expressed by

$$\tau_m = \mathbf{M}(q)\mathbf{J}^{-1}(q)\ddot{\mathbf{p}} + \mathbf{g}(q). \quad (5)$$

It should be noted that as the mapping relation is linear and the joint torque polytope is convex, the dynamic manipulability will hold the convex property. By mapping the 2^n vertices of the joint torque polytope, the vertices required for constructing the DMP is extracted, as shown in Fig. 3. At any given configuration, the DMP can therefore be computed from the $2n$ equations as follows

$$|\mathbf{M}(q)\mathbf{J}^{-1}(q)\ddot{\mathbf{p}} + \mathbf{g}(q)| \leq \tau_{max}. \quad (6)$$

While the computation of DMP vertices for a system with small number of degrees of freedom (DOFs) can be done manually, for systems with large number of DOFs, as well as for cases with high number of iterations such as this work, when employing Matlab[®] software, all mapped vertices can found using the “lcon2vert” function, when the above-said inequality (6) is expressed by $\mathbf{A}_a\ddot{\mathbf{p}} \leq \mathbf{b}_a$ with

$$\mathbf{A}_a = \begin{bmatrix} \mathbf{M}(q)\mathbf{J}^{-1}(q) \\ -\mathbf{M}(q)\mathbf{J}^{-1}(q) \end{bmatrix}, \quad \mathbf{b}_a = \begin{bmatrix} \tau_{max} - \mathbf{g}(q) \\ \tau_{max} + \mathbf{g}(q) \end{bmatrix}. \quad (7)$$

The DMP effective vertices can accordingly be extracted and sorted by means of the “convhull” function that also gives the area and the volume of the polytope in 2D and 3D space, respectively. The minimum distance from a given point and the 2D/3D, to be used for further computations, can then be

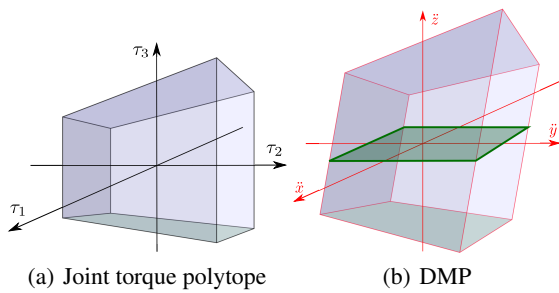


Figure 3: A sample representation of the joint torque polytope of a 3-DOF robot in a given configuration, and the corresponding dynamic manipulability polytope for the aforementioned task space definition, with its coincidence with the horizontal plane.

acquired by means of the “p_poly_dist” function. In this work, the task space position vector is defined by $\mathbf{p} = [x, y, z]^T$, and three indexes are defined as follows:

- The area of the DMP coincidence with the horizontal plane xy ; describing a criterion for overall acceleration in this plane: A_{xy} ,
- The ratio of the maximum to minimum acceleration in the horizontal plane xy ; subject to spatial translation of the DMP due to the gravitational torque; expressing the isotropy of acceleration in this plane: α_{xy} ,
- The ratio of the DMP volume to the area A_{xy} ; representing a measure for the acceleration along the vertical axis z : a_z .

3.4 Slippage Condition Index: Force Polytope

While the prior index focused on the free motion of the leg, this index evaluates the leg performance when applying external force on the end-effector due to the contact with ground. As the generation of thrust force on the robot requires the leg end-effector to avoid slipping on the ground, the third criterion studies the slippage condition of the leg. The necessary and sufficient requirement for preventing an object from slipping on a surface is to apply an adequately large normal force that satisfies

$$\frac{F_t}{F_n} \leq \mu_s, \quad (8)$$

where F_t and F_n represent the tangential and normal forces, respectively, and μ_s is the static friction coefficient of the contact surface.

It is therefore suitable to design the robot leg in such a way that the highest ratio of normal force to tangential force on the end-effector can be achieved, and the locomotion on a wider frictional range for

ground surfaces can be feasible. To achieve this, and considering the higher accuracy obtained from force polytope when compared to that from force ellipsoid, the evolution of the normal force to tangential force ratio is studied by means of force polytope. Based on the actuator torque limits (4) presenting the joint torque polytope, according to (Chiacchio et al., 1997), the force polytope can be found when the joint torque to the end-effector force mapping is applied as follows

$$\boldsymbol{\tau}_m = \mathbf{J}^T \mathbf{F}_{ext}. \quad (9)$$

The force polytope can therefore be computed by implementing the same procedure as the DMP. By applying the torque limit (4) on the above-said torque-force mapping (9), the force polytope vertices are extracted from $\mathbf{A}_f \mathbf{F}_{ext} \leq \mathbf{b}_f$ with

$$\mathbf{A}_f = \begin{bmatrix} \mathbf{J}^T(\mathbf{q}) \\ -\mathbf{J}^T(\mathbf{q}) \end{bmatrix}, \quad \mathbf{b}_f = \begin{bmatrix} \tau_{max} \\ \tau_{max} \end{bmatrix}, \quad (10)$$

while \mathbf{b}_f is replaced by \mathbf{b}_a when the gravitational translation of the polytope is taken into account.

As the robot body is assumed to be placed in parallel with the ground, the tangential element F_t is the external force in the horizontal plane, while the normal element F_n is the force along the vertical axis. To demonstrate the variation in normal force to tangential force ratio, the index β is defined based on the volume of the force polytope V_f , the area of the force polytope coincidence with the horizontal plane A_t , and the maximum tangential force F_{mt} as follows

$$\beta = \frac{V_f}{\frac{A_t}{F_{mt}}}. \quad (11)$$

4 SIMULATION ANALYSIS

In this section, the numerical simulations of two legs based on the two kinematics arrangements are carried out. For this comparison, the mass and length of the leg links attached to the afore-stated joints are assumed to be as follows: The bar linking the hip roll/yaw joint to the hip pitch joint is $0.1\sqrt{2}$ m long, including 0.1 m offset and 0.1 m normal length, with a mass of 2 Kg, the link connecting the hip pitch joint to the knee joint has a length of 0.4 m and a mass of 4.5 Kg, and the last link attached to the knee joint is 0.4 m long with a mass of 3.5 Kg. The body mass is considered to be 80 Kg. To facilitate the presentation of results, the simulations are carried out in three cases when the robot body is positioned at three heights, and the Cartesian motion of the end-effector is confined with three half-circles as follows: I) at the height of 0.3 m, with a half-circle of radius 0.5 m,

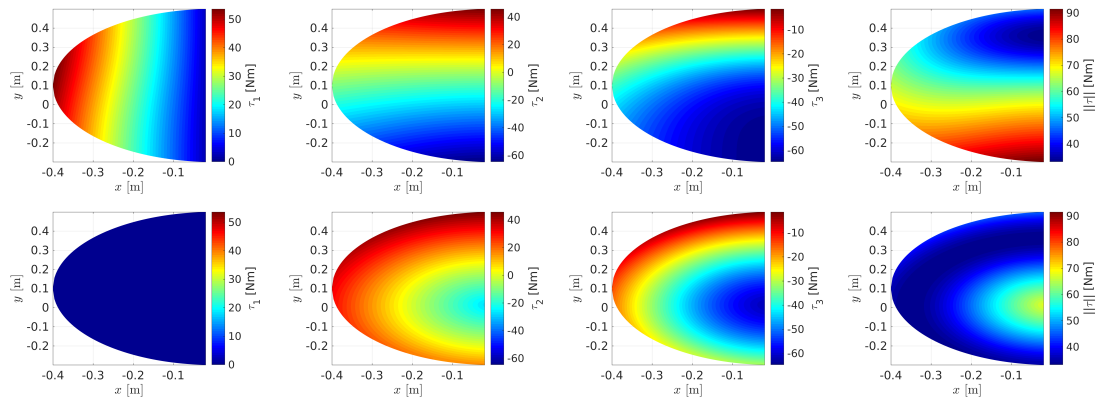


Figure 4: The evolution of gravity compensation torque in xy-plane when the robot is set in different configurations within the defined workspace II, while standing on a horizontal plane $\gamma = 0$, for two kinematics arrangement: The RPP torques at the first row, and the YPP torques at the bottom.

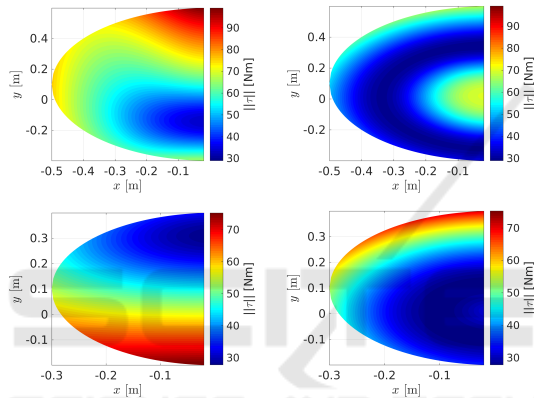


Figure 5: The evolution of gravity compensation torque in xy-plane when the robot is set in different configurations within the defined workspace I and III, while standing on a horizontal plane $\gamma = 0$, for two kinematics arrangement: The RPP torques on the left side, and the YPP torques on the right side.

II) at the height of 0.5 m, with a half-circle of radius 0.4 m, III) at the height of 0.7 m, with a half-circle of radius 0.3 m.

Fig. 4 presents the evolution of the gravity compensation torque within the workspace defined in case II, for the both leg arrangements when standing on a horizontal plane, $\gamma = 0$. It illustrates the torque corresponding to individual joints, as well as the L^2 -norm of the torque vector. It can be seen that, when the robot operates on a horizontal plane, the gravity compensation torques of the hip and knee pitch joints vary within similar ranges, whereas the first joints of the two arrangements exhibit differently. While the hip roll joint demands a considerable amount of torque, the hip yaw joint needs a negligible torque. The resulting torque norm of the YPP arrangement is therefore larger than that of the RPP arrangement. Such a difference can be also seen in

Table 1: Maximum gravity compensation torque for various cases (values are in Nm).

| | | τ_1 | τ_2 | τ_3 | $\ \tau\ $ | |
|----------|-----|---------------------|----------|----------|------------|----|
| Case I | RPP | $\gamma = 0$ | 74 | 75 | 65 | 99 |
| | | $\gamma = 30^\circ$ | 42 | 73 | 65 | 97 |
| | YPP | $\gamma = 0$ | 0 | 63 | 65 | 70 |
| | | $\gamma = 30^\circ$ | 36 | 54 | 65 | 70 |
| Case II | RPP | $\gamma = 0$ | 54 | 65 | 65 | 91 |
| | | $\gamma = 30^\circ$ | 34 | 60 | 64 | 88 |
| | YPP | $\gamma = 0$ | 0 | 45 | 62 | 67 |
| | | $\gamma = 30^\circ$ | 28 | 49 | 65 | 80 |
| Case III | RPP | $\gamma = 0$ | 40 | 50 | 55 | 75 |
| | | $\gamma = 30^\circ$ | 46 | 45 | 51 | 78 |
| | YPP | $\gamma = 0$ | 0 | 65 | 32 | 70 |
| | | $\gamma = 30^\circ$ | 28 | 56 | 56 | 68 |

the results corresponding to the workspaces defined in case I and III, reported in Fig. 5 (As for the cases I and III, for the sake of brevity, only the norm of the torque vector is reported here). However, when the robot stands on an inclined surface with a slope of $\gamma = 30^\circ$, see Figs. 6 and 7, the difference between the maximum torque required for the first joints significantly decrease. Nevertheless, the torque threshold associated with the first hip joint of the YPP arrangement, as well as the torque vector norm, remains lower than that of the RPP arrangement.

The maximum torque value corresponding to the different cases are reported in Table 1, demonstrating lower joint torques for the spider-like leg (YPP arrangement), as compared to the mammal-like leg (RPP arrangement). Based on these values, the torque limit of joints are set to $\tau_{max} = (75, 75, 65)$ Nm for the further manipulability analysis.

The evolution of the DMP indexes within the workspace cases I and III are illustrated in Figs. 8 and 9, respectively. It can be observed from Fig. 8 that, when the robot body is relatively close

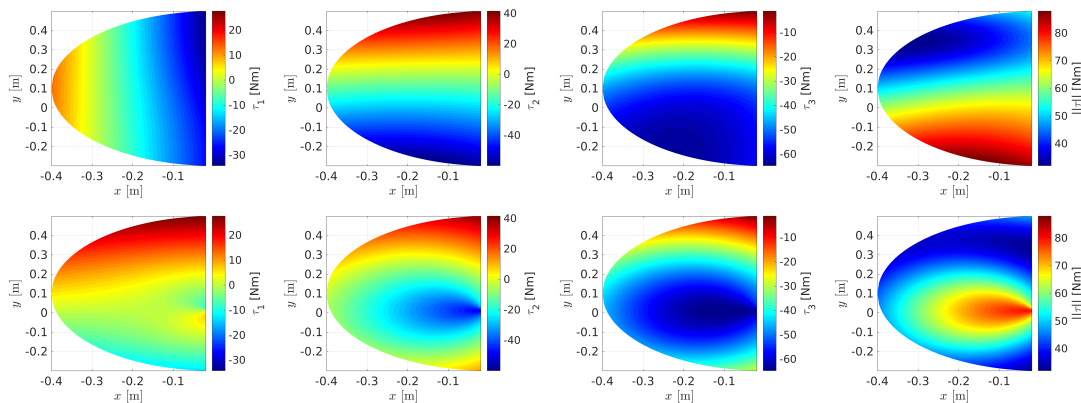


Figure 6: The evolution of gravity compensation torque in xy-plane when the robot is set in different configurations within the defined workspace II, while standing on an inclined plane $\gamma = 30^\circ$, for two kinematics arrangement: The RPP torques at the first row, and the YPP torques at the bottom.

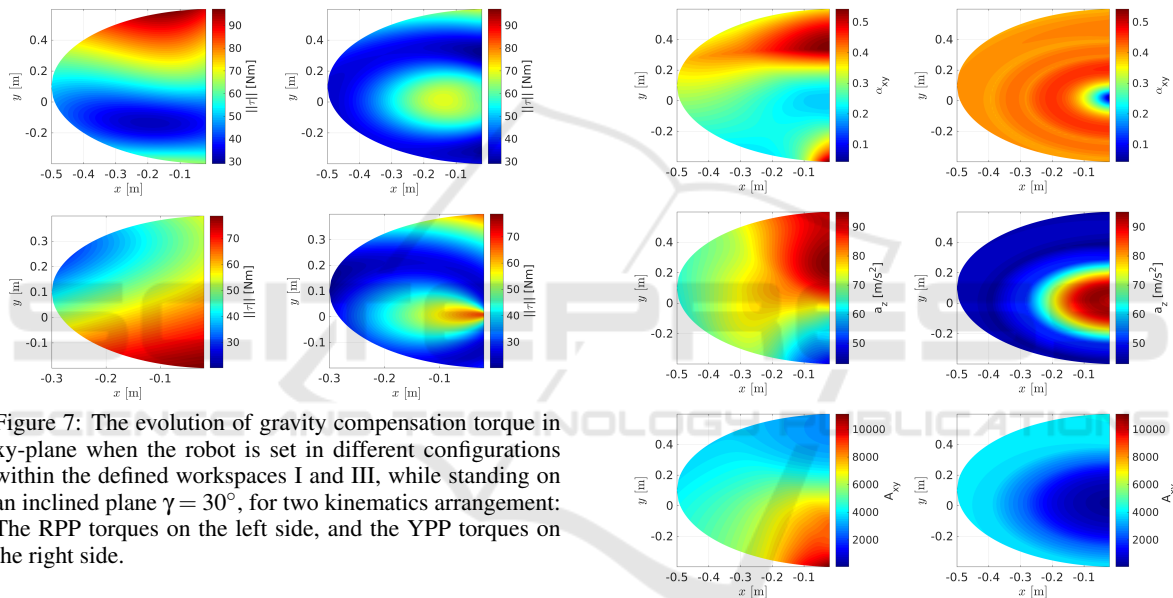


Figure 7: The evolution of gravity compensation torque in xy-plane when the robot is set in different configurations within the defined workspaces I and III, while standing on an inclined plane $\gamma = 30^\circ$, for two kinematics arrangement: The RPP torques on the left side, and the YPP torques on the right side.

to the ground, the spider-like leg can possess a higher level of dynamic manipulability isotropy than the mammal-like leg; however, in terms of the DMP magnitude in xy-plane, presented by A_{xy} , the spider-like leg cannot show a better performance than the mammal-like leg. On the other hand, when the robot body is set to be in a higher distance from the ground, i.e. the case III as depicted in Fig. 9, the mammal-like leg exhibits higher dynamic manipulability isotropy with lower magnitude A_{xy} , as compared to the spider-like leg. Regarding the dynamic manipulability along the vertical axis, represented by a_z , the mammal-like leg provides larger end-effector accelerations than the other leg arrangement in a majority of configurations.

The evaluation of the slippage condition index β for the two leg kinematics arrangements is illustrated in Fig. 10. It can be seen that when the robot

Figure 8: The evolution of the DMP indexes in xy-plane when the robot is set in different configurations within the defined workspace I, for two kinematics arrangement: The RPP torques on the left side, and the YPP torques on the right side.

body is not positioned close to the ground (case III), the mammal-like leg (RPP arrangement) allows locomotion on more slippery surfaces, as compared to the spider-like leg (YPP arrangement). However, the spider-like leg can render motions on more slippery surfaces when the robot is configured to hold its body close to the ground (case I), although it is not valid everywhere in the defined workspace. When the robot body is set in a position between the two above-said cases (case II), the two RPP and YPP arrangements exhibit similar performances when the leg end-effector is not radially close to the hip joint, while the mammal-like leg may possess better

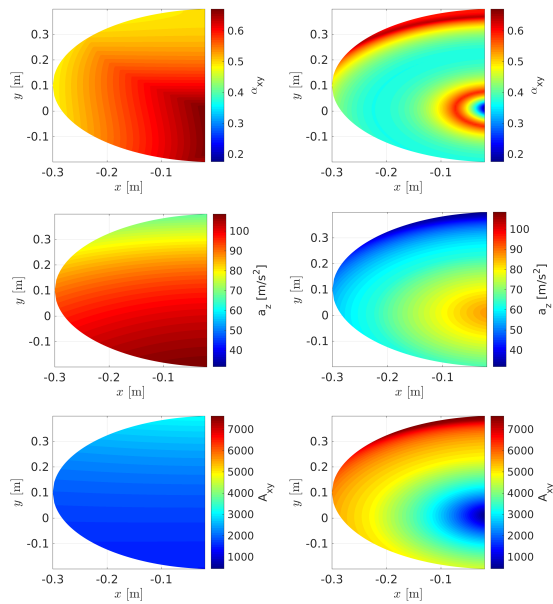


Figure 9: The evolution of the DMP indexes in xy -plane when the robot is set in different configurations within the defined workspace III, for two kinematics arrangement: The RPP torques on the left side, and the YPP torques on the right side.

slippage avoidance capacity when the leg end-effector radially approaches the first joint.

5 CONCLUSIONS

This work presented a comparison study for the leg kinematics arrangement of a quadrupedal robot, on the basis of two conventional leg configurations inspired by the skeleton of mammals and spiders/insects. The statics and dynamics performances of the two arrangements are evaluated by defining some criteria including the minimum torque capacity of joints, the responsive/reactive motion of legs, and the slippage avoidance condition. To this end, a set of indexes are defined based on the gravity compensation torque of joints, the dynamic manipulability polytope and the force manipulability polytope. Eventually, the simulation results describing the evolution of the performance indexes within a set of workspaces are illustrated.

The results revealed the lower torque requirement of the spider-like leg as compared to the mammal-like leg, resulting from the perpendicularity of its first joint axis to the ground. It was also seen that the mammal-like leg benefits from higher dynamic manipulability isotropy when the leg is nearly straight and the robot body is close to its maximum distance from the ground. In such a posture, the mammal-like

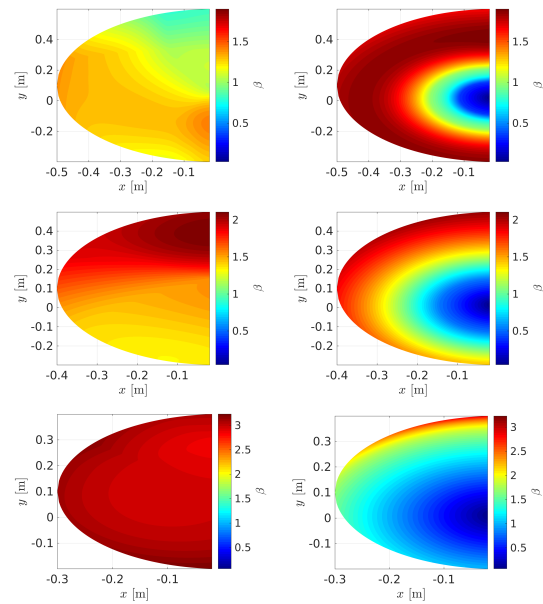


Figure 10: The evolution of the slippage avoidance index in xy -plane when the robot is set in different configurations within the defined workspace I, II and III, presented at the first, second and third row, respectively; while the two kinematics arrangement RPP and YPP are shown on the left and right sides.

leg can also handle slippery surface better than the spider-like leg. On the other hand, the spider-like leg can possess larger dynamic manipulability isotropy, and avoid slippage on more slippery surfaces, when the robot body is positioned close to ground. The mammal-like legs can therefore be selected when straight leg dynamic motions are desired, while the spider-like legs may be chosen if the execution of high power tasks demanding large support polygon and close-to-ground centre of mass is needed.

Future work of the authors may analyse the leg performance when the passive/active impedance of joints is taken into account (Laffranchi et al., 2014; Kashiri et al., 2014; Spyarakos-Papastavridis et al., 2015).

ACKNOWLEDGEMENTS

This project has received funding from the European Union's Horizon 2020 research and innovation programme under grant agreement Centauro No 644839 (ICT-23-2014 Robotics).

REFERENCES

- Bagheri, M., Ajoudani, A., Lee, J., Caldwell, D. G., and Tsagarakis, N. G. (2015). Kinematic Analysis and Design Considerations for Optimal Base Frame Arrangement of Humanoid Shoulders. In *IEEE Int. Conf. Robot. Autom.*, pages 2710–2715, Seattle.
- Belter, D., Skrzypczyński, P., Walas, K., and Wlodkowic, D. (2015). Affordable Multi-legged Robots for Research and STEM Education: A Case Study of Design and Technological Aspects. In *Prog. Autom. Robot. Meas. Tech.*, pages 23–34. Springer.
- Caldwell, D. G., Tsagarakis, N., and Semini, C. (2014). Mechanism and Structures: Humanoids and Quadrupeds. In *Bioinspired Approaches for Human-Centric Technologies*, pages 133–153.
- Chen, J. J., Peattie, A. M., Autumn, K., and Full, R. J. (2006). Differential leg function in a sprawled-posture quadrupedal trotter. *J. Exp. Biol.*, 209(2):249–259.
- Chen, X., Sun, Y., Huang, Q., Jia, W., and Pu, H. (2008). Development of Multi-Legged Walking Robot Using Reconfigurable Modular Design and Biomimetic Control Architecture. *J. Syst. Des. Dyn.*, 2(1):401–412.
- Chiacchio, P., BouffardVercelli, Y., and Pierrot, F. (1997). Force polytope and force ellipsoid for redundant manipulators. *J. Robot. Syst.*, 14(8):613–620.
- Corke, P. (2011). *Robotics, Vision and Control: Fundamental Algorithms in MATLAB*. Springer Science & Business Media.
- Gasparetto, A., Vidoni, R., and Seidl, T. (2008). Kinematic study of the spider system in a biomimetic perspective. In *IEEE/RSJ Int. Conf. Intell. Robot. Syst.*, pages 3077–3082. IEEE.
- Ho, T., Choi, S., and Lee, S. (2007). Development of a biomimetic quadruped robot. *J. Bionic Eng.*, 4(4):193–199.
- Hutter, M., Gehring, C., Bloesch, M., Hoepflinger, M. A., Remy, C. D., and Siegwart, R. (2012). StarIETH: A compliant quadrupedal robot for fast, efficient, and versatile locomotion. In *15th Int. Conf. Climbing Walk. Robot. 2012*, number EPFL-CONF-181042.
- Kang, T., Kim, H., Son, T., and Choi, H. (2003). Design of quadruped walking and climbing robot. In *IEEE/RSJ Int. Conf. Intell. Robot. Syst.*, volume 1, pages 619–624. IEEE.
- Kar, D. C. (2003). Design of statically stable walking robot: a review. *J. Robot. Syst.*, 20(11):671–686.
- Kashiri, N., Tsagarakis, N. G., Van Damme, M., Vanderborght, B., and Caldwell, D. G. (2014). Enhanced Physical Interaction Performance for Compliant Joint Manipulators using Proxy-based Sliding Mode Control. In *Int. Conf. Informatics Control. Autom. Robot.*, pages 175–183, Vienna.
- Kato, K. and Hirose, S. (2001). Development of the quadruped walking robot, TITAN-IXmechanical design concept and application for the humanitarian de-mining robot. *Adv. Robot.*, 15(2):191–204.
- Laffranchi, M., Chen, L., Kashiri, N., Lee, J., Tsagarakis, N. G., and Caldwell, D. G. (2014). Development and control of a series elastic actuator equipped with a semi active friction damper for human friendly robots. *Rob. Auton. Syst.*, 62(12):1827–1836.
- Negrello, F., Garabini, M., Catalano, M. G., Kryczka, P., Choi, W., Caldwell, D. G., Bicchi, A., and Tsagarakis, N. G. (2016). WALK-MAN Humanoid Lower body Design Optimization for Enhanced Physical Performance. In *IEEE Int. Conf. Robot. Autom.*, Stockholm.
- Pratt, J. E. and Tedrake, R. (2006). Velocity-based stability margins for fast bipedal walking. In *Fast Motions Biomech. Robot.*, pages 299–324. Springer.
- Raibert, M., Blankespoor, K., Nelson, G., Playter, R., and Team, T. B. (2008). Bigdog, the rough-terrain quadruped robot. In *Proc. 17th World Congr.*, volume 17, pages 10822–10825.
- Roennau, A., Heppner, G., Pfozter, L., and Dillman, R. (2013). Lauron V: Optimized leg configuration for the design of a bio-inspired walking robot. In *Proc. 16th Int. Conf. Climbing Walk. Robot. Support Technol. Mob. Mach.*, volume 1417.
- Semini, C., Tsagarakis, N. G., Guglielmino, E., Focchi, M., Cannella, F., and Caldwell, D. G. (2011). Design of HyQa hydraulically and electrically actuated quadruped robot. *Proc. Inst. Mech. Eng. Part I J. Syst. Control Eng.*, page 0959651811402275.
- Seok, S., Wang, A., Chuah, M. Y., Otten, D., Lang, J., and Kim, S. (2013). Design principles for highly efficient quadrupeds and implementation on the MIT Cheetah robot. In *IEEE Int. Conf. Robot. Autom.*, pages 3307–3312. IEEE.
- Shkolnik, A., Levashov, M., Manchester, I. R., and Tedrake, R. (2010). Bounding on rough terrain with the LittleDog robot. *Int. J. Rob. Res.*, page 0278364910388315.
- Siciliano, B., Sciavicco, L., Villani, L., and Oriolo, G. (2009). *Robotics: Modelling, Planning and Control*. Springer Science & Business Media.
- Spröwitz, A., Tuleu, A., Vespignani, M., Ajallooeian, M., Badri, E., and Ijspeert, A. J. (2013). Towards dynamic trot gait locomotion: Design, control, and experiments with Cheetah-cub, a compliant quadruped robot. *Int. J. Rob. Res.*, 32(8):932–950.
- Spyrakos-Papastavridis, E., Kashiri, N., Lee, J., Tsagarakis, N. G., and Caldwell, D. G. (2015). Online impedance parameter tuning for compliant biped balancing. In *IEEE-RAS International Conference on Humanoid Robots*, pages 210–216.
- Xie, H., Zhang, Z., Shang, J., and Luo, Z. (2014). Mechanical Design of A Modular Quadruped Robot-XDog. In *Int. Conf. Mechatronics, Electron. Ind. Control Eng.*, pages 1074–1078.
- Yoshikawa, T. (1985). Dynamic manipulability of robot manipulators. In *IEEE Int. Conf. Robot. Autom.*, volume 2, pages 1033–1038. IEEE.
- Zielinska, T. (2013). Design Issues and Robots Autonomy. In *New Trends Mech. Mach. Sci.*, pages 691–699.
- Zielinska, T. and Heng, J. (2003). Mechanical design of multifunctional quadruped. *Mech. Mach. Theory*, 38(5):463–478.